Supplementary Information (SI) for Journal of Materials Chemistry C.

SUPPORTING INFORMATION

High-efficiency self-powered perovskite photodetector with electron-enhancing SnO_2/WS_2 double electron transport layer

Vo Pham Hoang Huy, Chung Wung Bark[1,*]

[1]Department of Electrical Engineering, Gachon University, Seongnam, Gyeonggi 13120, Republic of Korea.

*Correspondence: bark@gachon.ac.kr

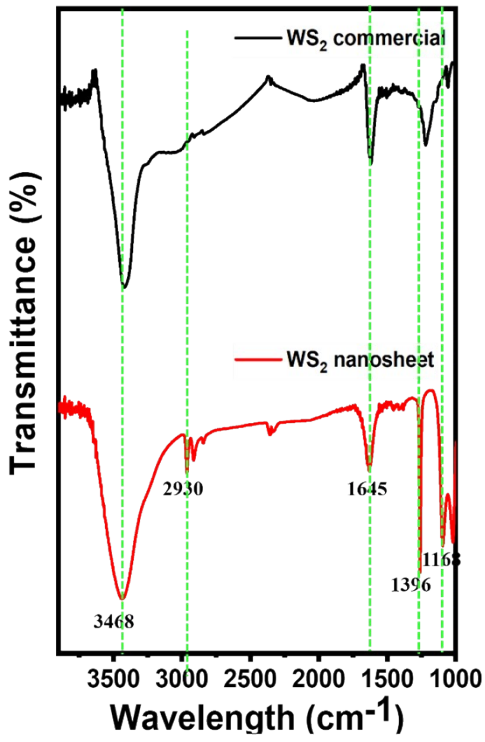

Fig. S1. FT-IR of WS_2 commercial and WS_2 nanosheet

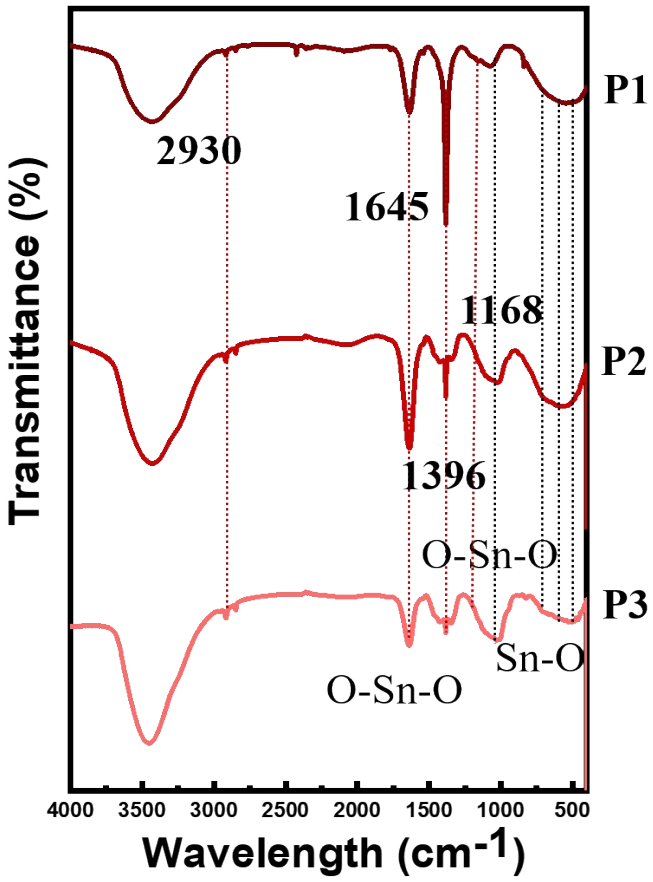

Fig. S2. FTIR of SnO_2-WS_2 at P1, P2, and P3 conditions

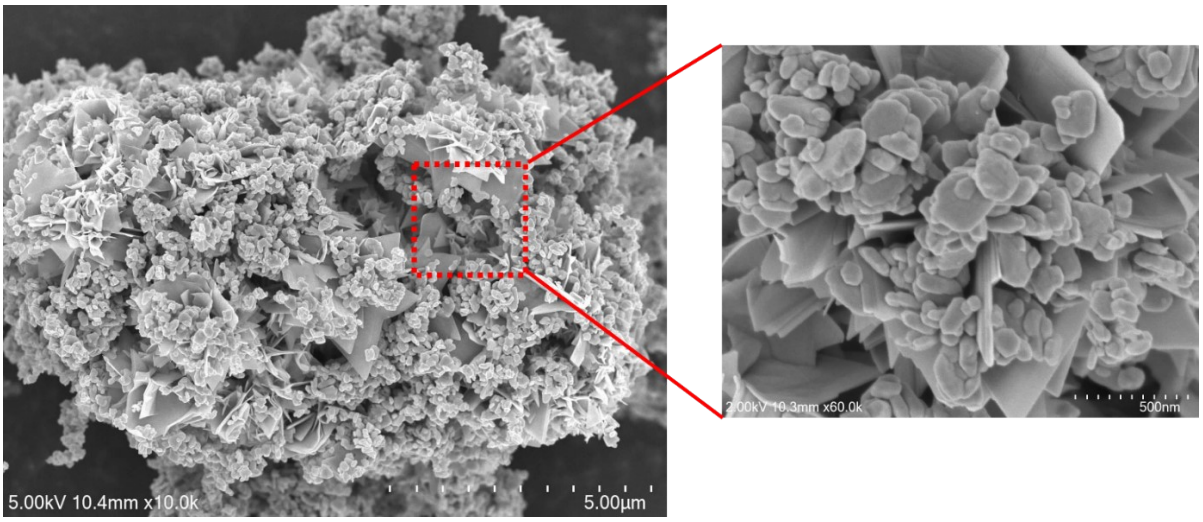

Fig. S3. SEM image of WS_2 commercial

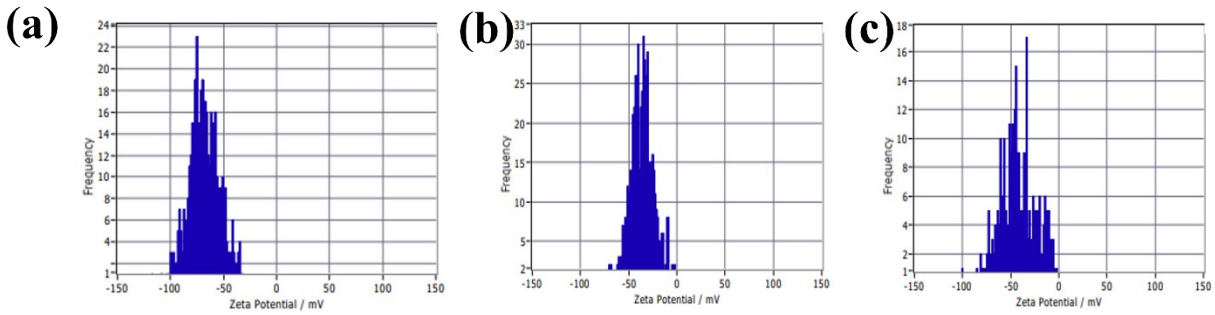

Fig. S4. Zeta potential of (a) SnO_2, (b) WS_2, (c)SnO_2-WS_2

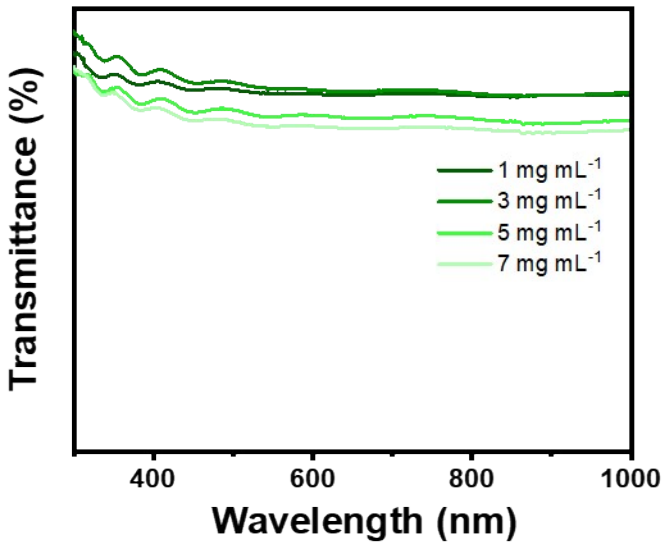

Fig. S5. Transmittance of WS_2 at different concentrations.

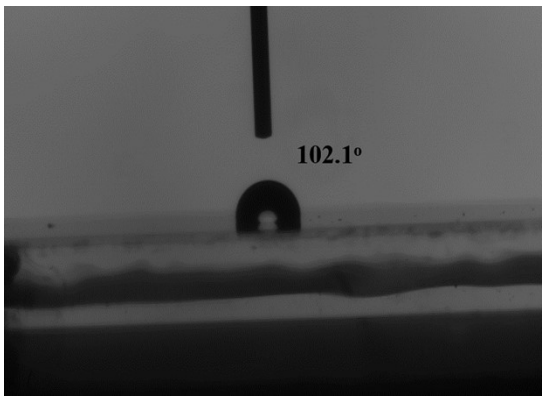

Fig. S6. Contact angel measurment of WS_2

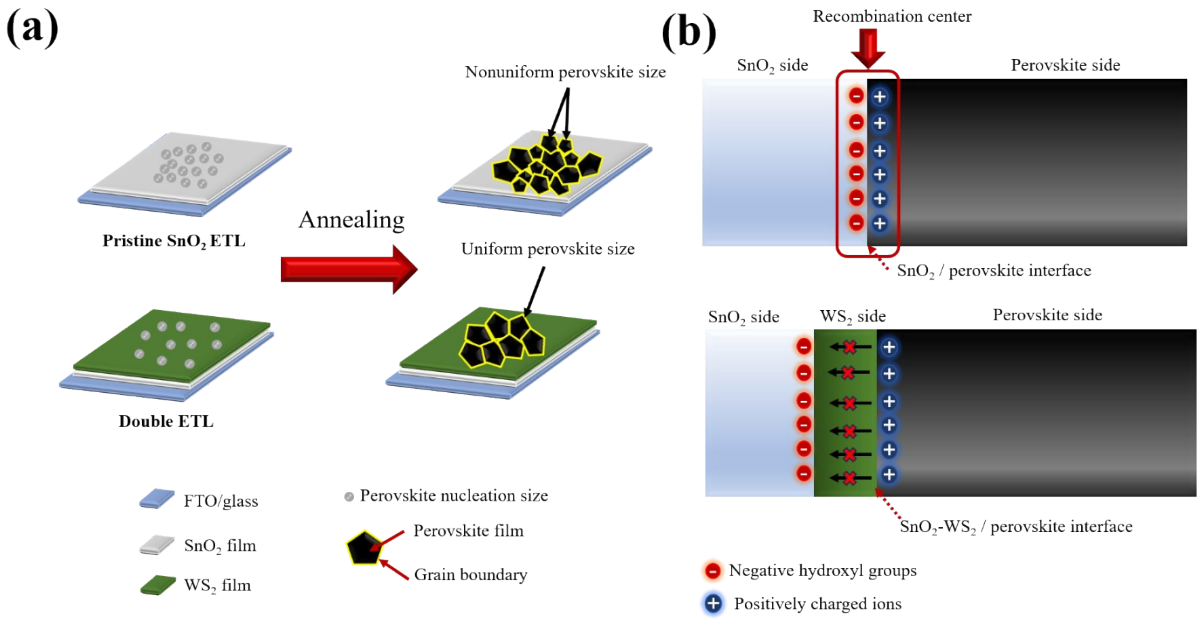

Fig. S7. (a) Schematic illustration of the nucleation of perovskite on pristine SnO_2 and SnO_2/WS_2 ETL, (b) Schematic illustration of the formation of recombination center between negative hydroxyl groups from SnO_2 side and positively charge ions from perovskite in the structure with and without the presence of WS_2

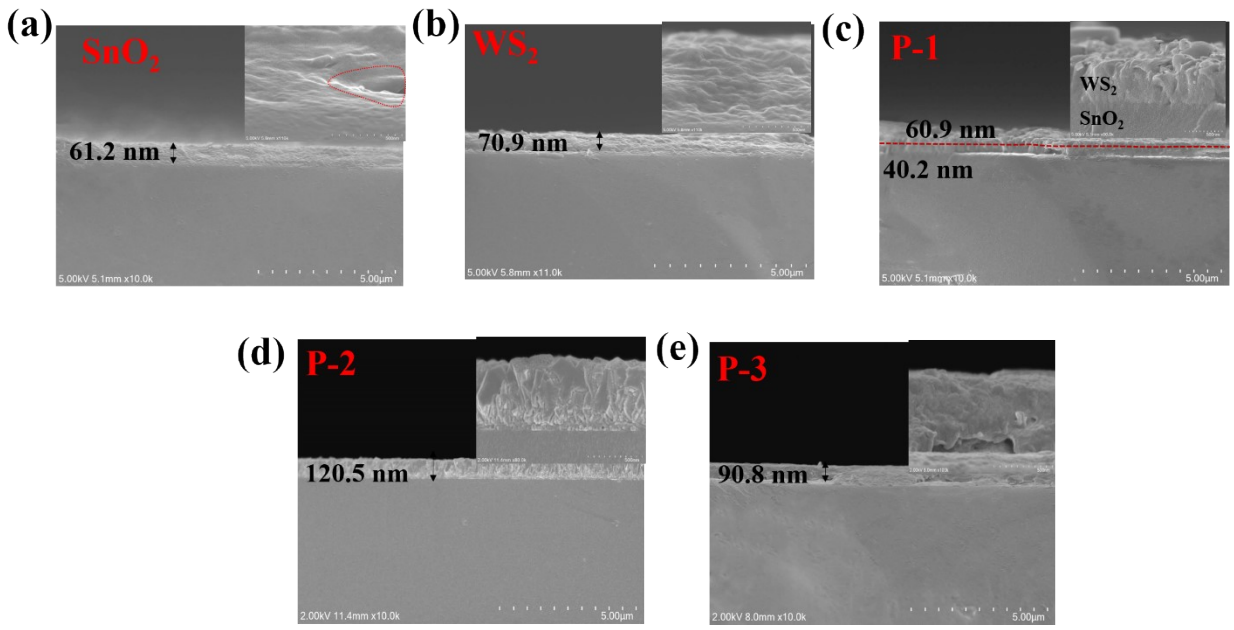

Fig. S8. (a) Cross-section SEM image of (a) FTO/SnO_2, (b) FTO/WS_2, (c) FTO/SnO_2-WS_2 (P1), (d) FTO/SnO_2-WS_2 (P2), (e) FTO/SnO_2-WS_2 (P3)

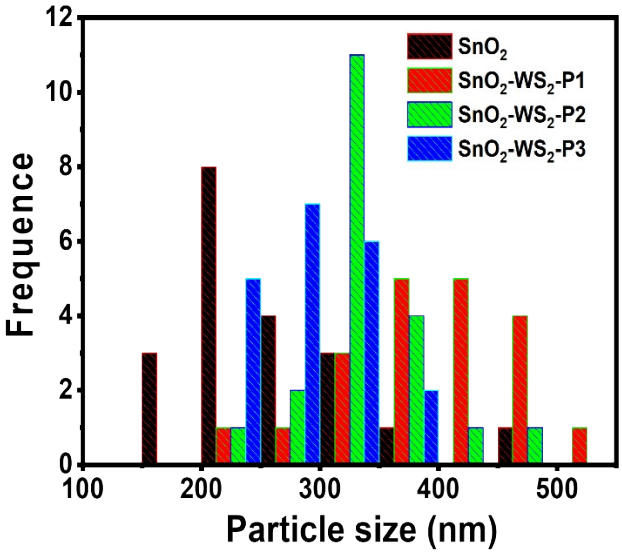

Fig. S9. Particle size distribution on SnO_2, SnO_2-WS_2 (P1), SnO_2-WS_2 (P2), and SnO_2-WS_2 (P3)

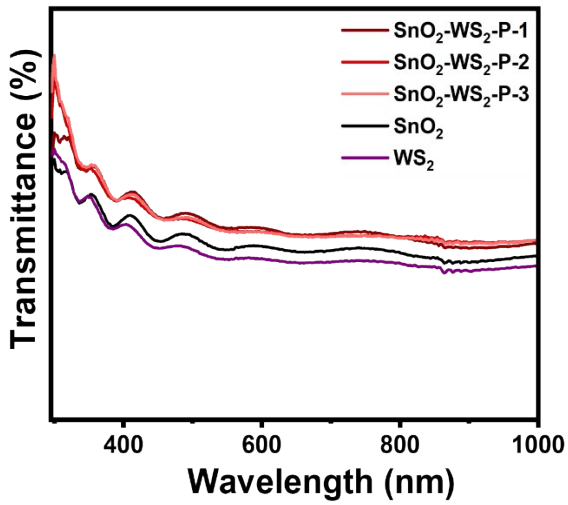

Fig. S10. Transmittance of SnO_2, WS_2, SnO_2-WS_2 (P1), SnO_2-WS_2 (P2), and SnO_2-WS_2 (P3)

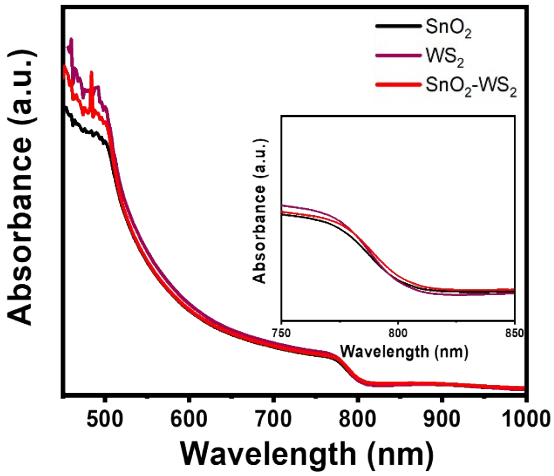

Fig. S11. Absorbance of perovskite on different ETLs

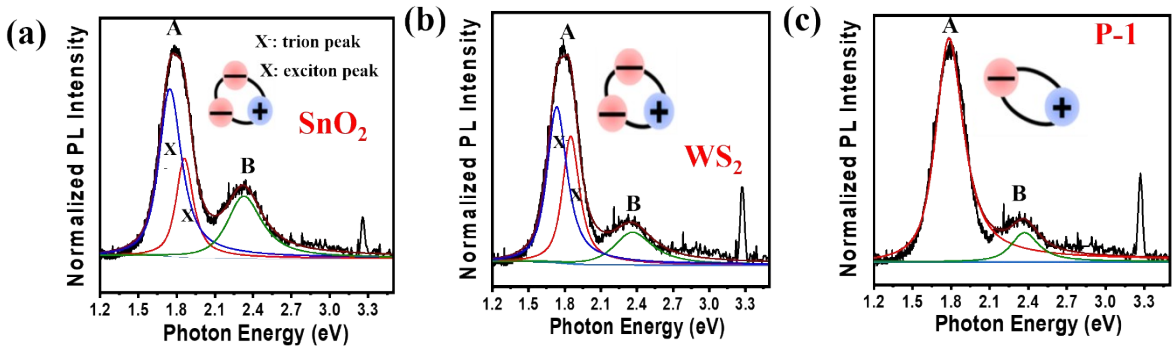

Fig. S12. Analysis of the PL spectral shapes for (a) SnO_2, (b) WS_2, and (c)as-prepared SnO_2-WS_2-P1. The A peaks in the PL spectra were reproduced by assuming two peaks with Lorentzian functions, corresponding to the trion (X−) and the exciton (X) peaks.

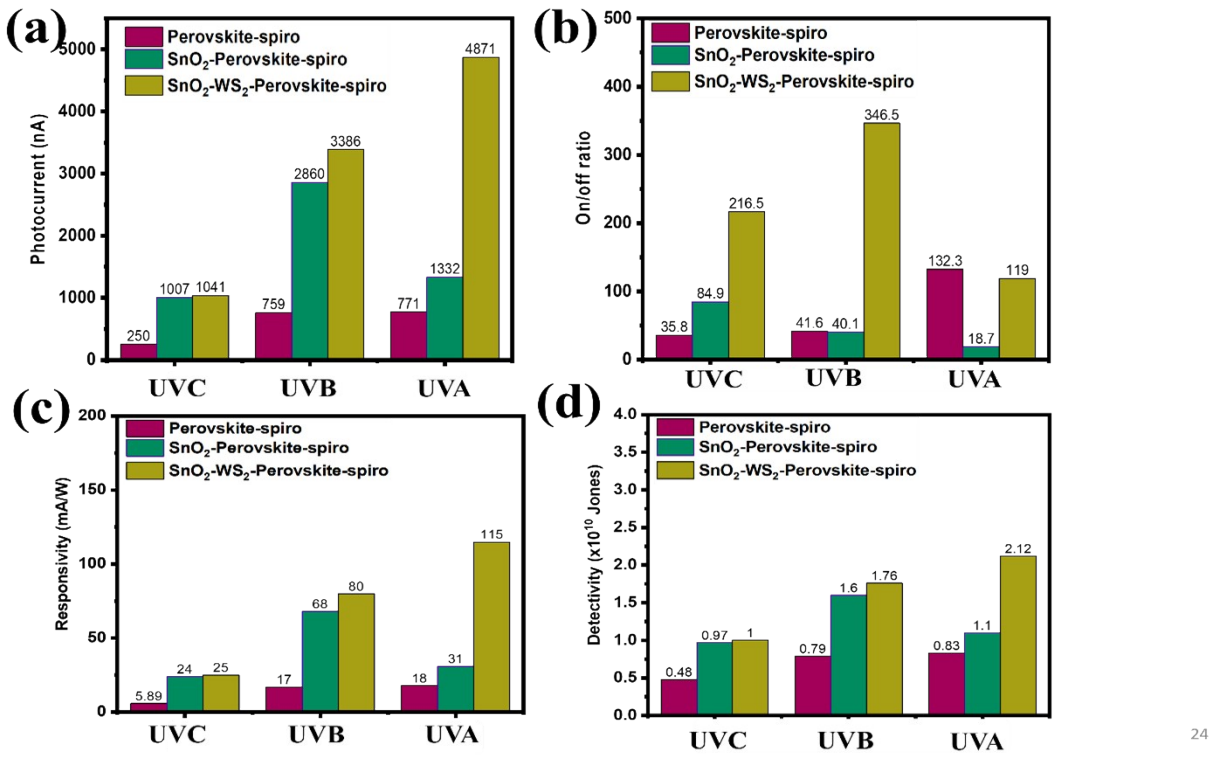

Fig. S13. The performance of different PD devices with (a) Time-domain response (b) on/off rato, (c) responsivity , and (d) detectivity

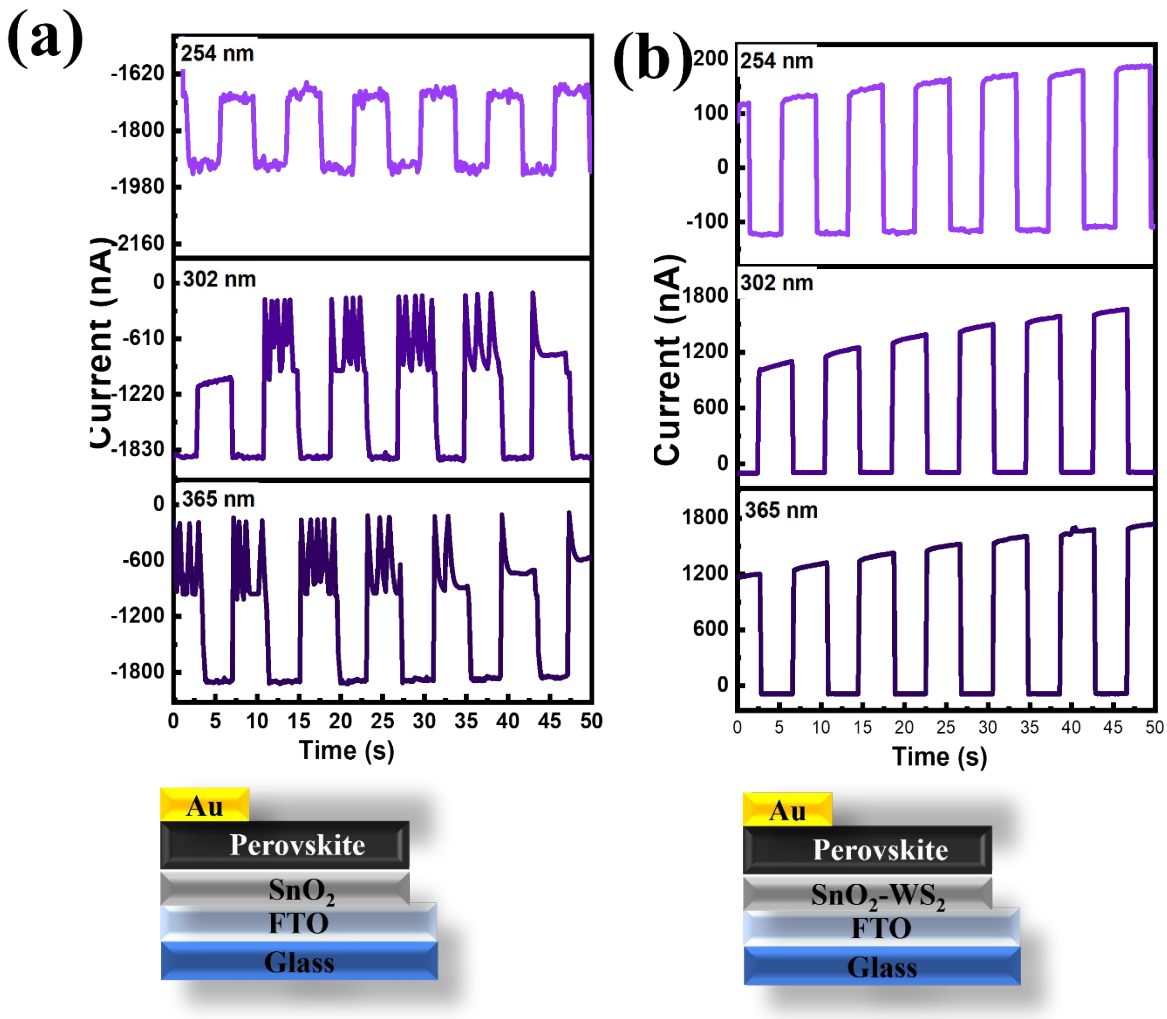

Fig. S14. Time-domain response of different PD device without HTL

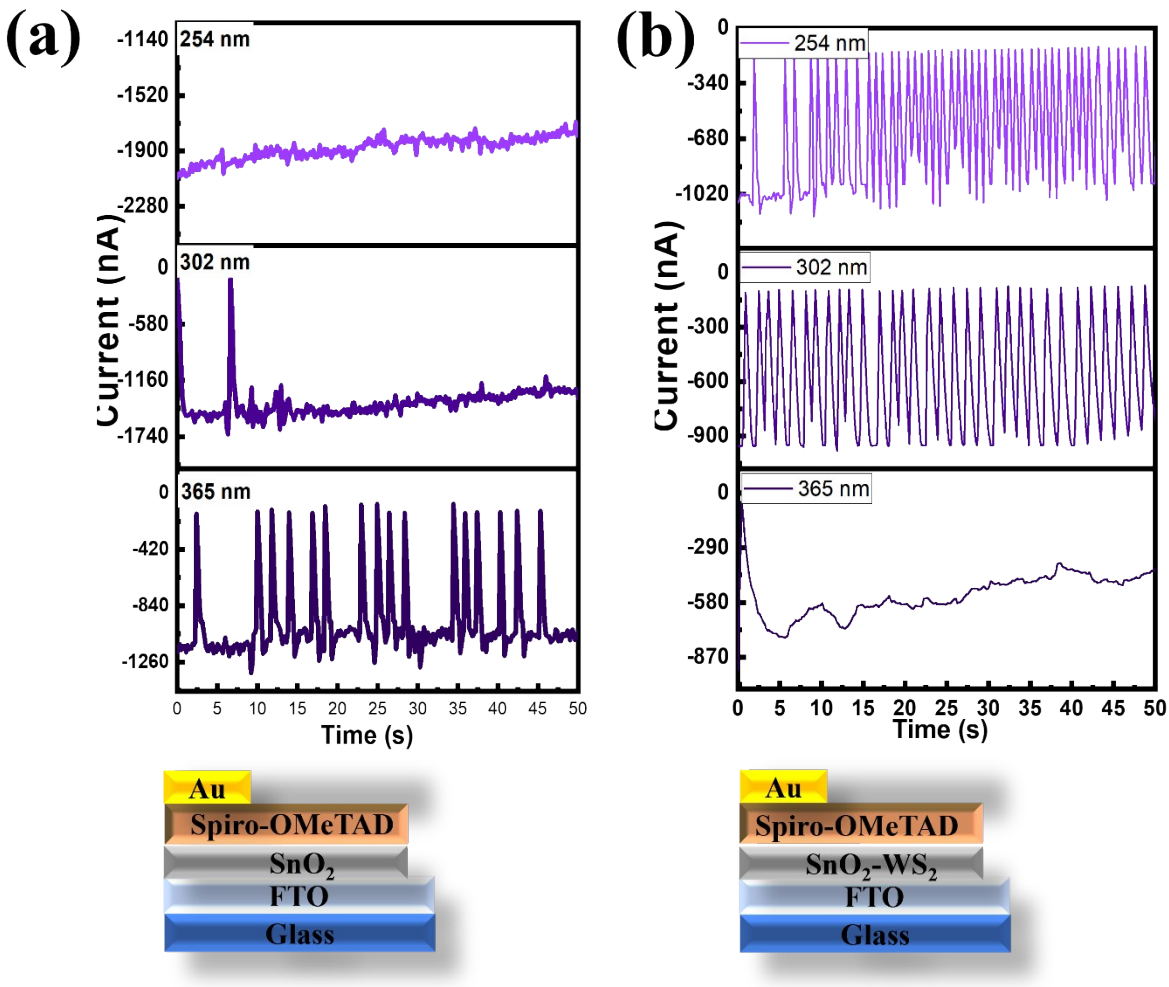

Fig. S15. Time-domain response of different PD device without photoactive

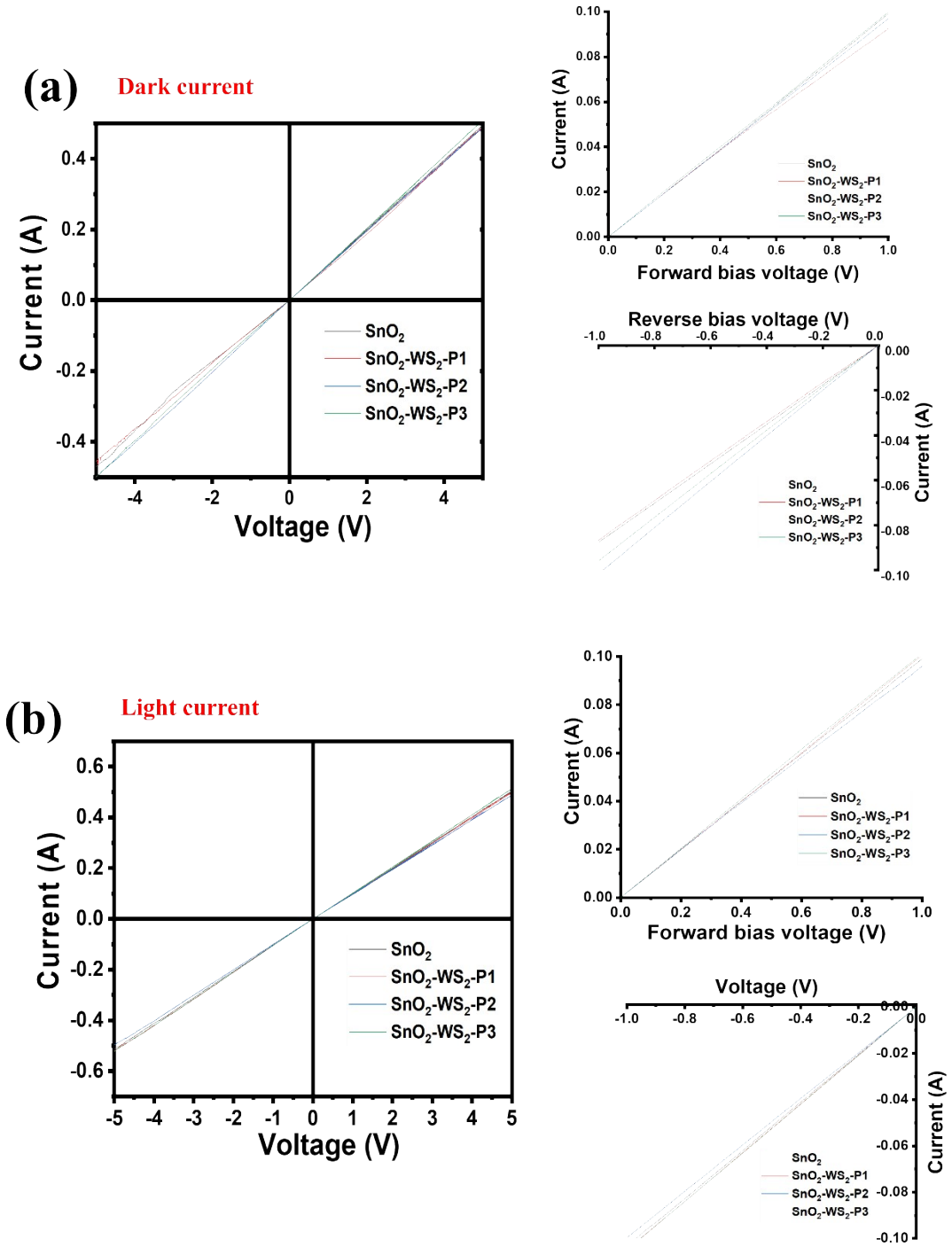

Fig. S16. I-V curves of different ETL at (a) a dark environment and (b) under 254 nm irradiation

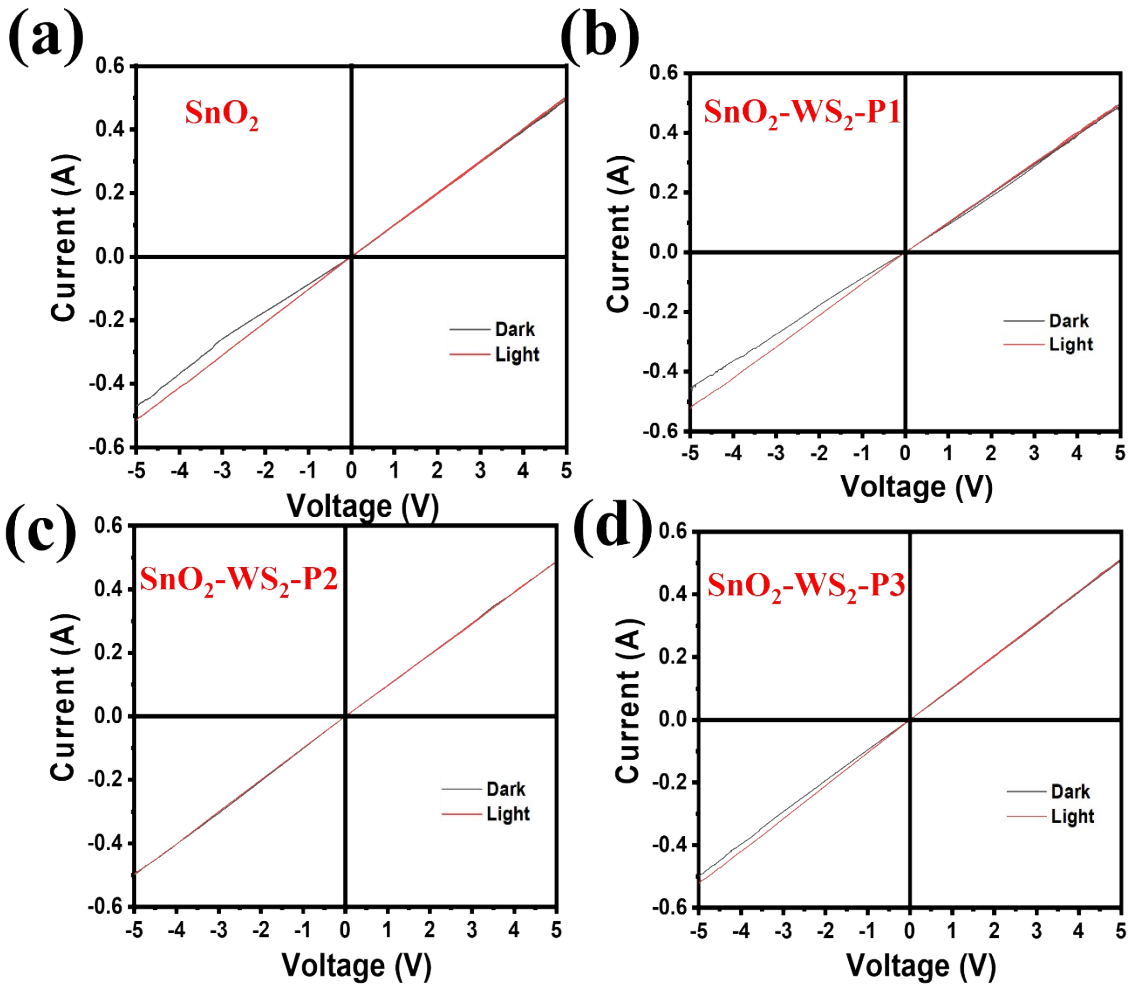

Fig. S17. I-V curves of PD devices at different ETL at (a) a dark environment and (b) under 254 nm irradiation

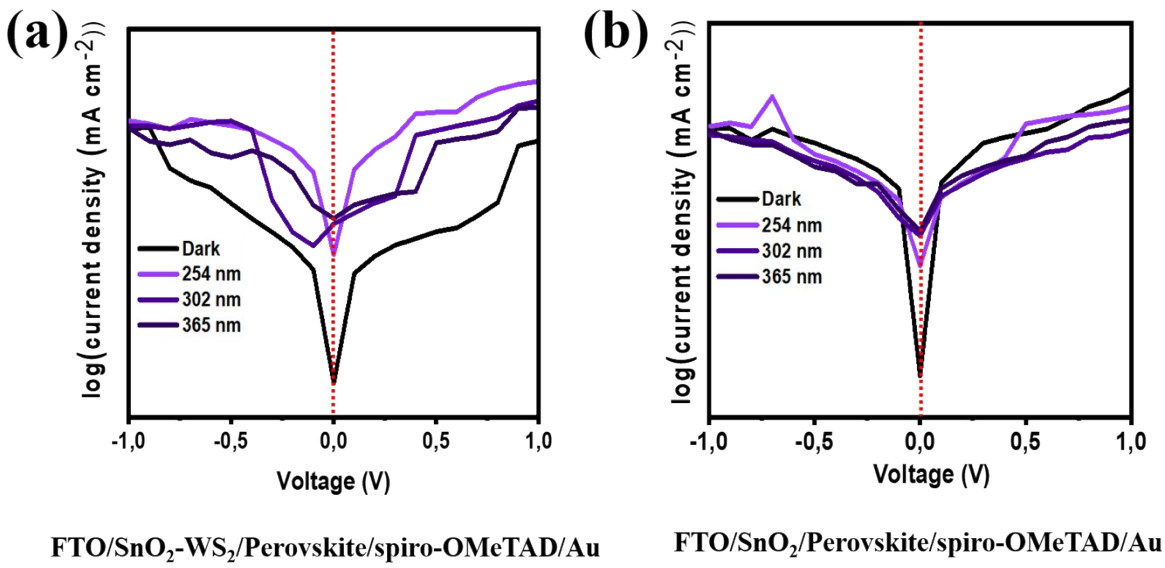

Fig. S18. J-V curves of PD devices at different ETL in a dark environment and under 254 nm, 302 nm, and 365 nm radiation.

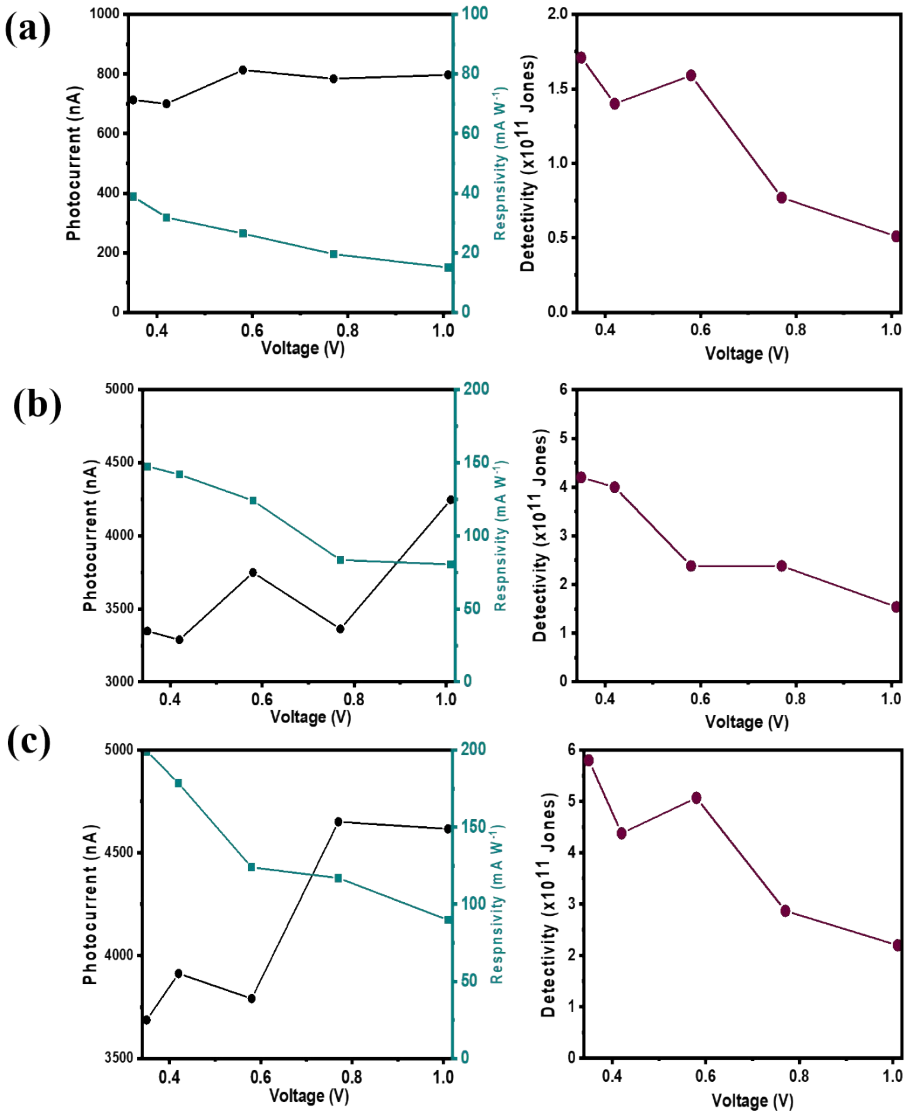

Fig. S19. The performance of different PD devices with photocurrent, responsivity , and detectivity of (a) UVC, (b) UVB, and (c) UVA regions.

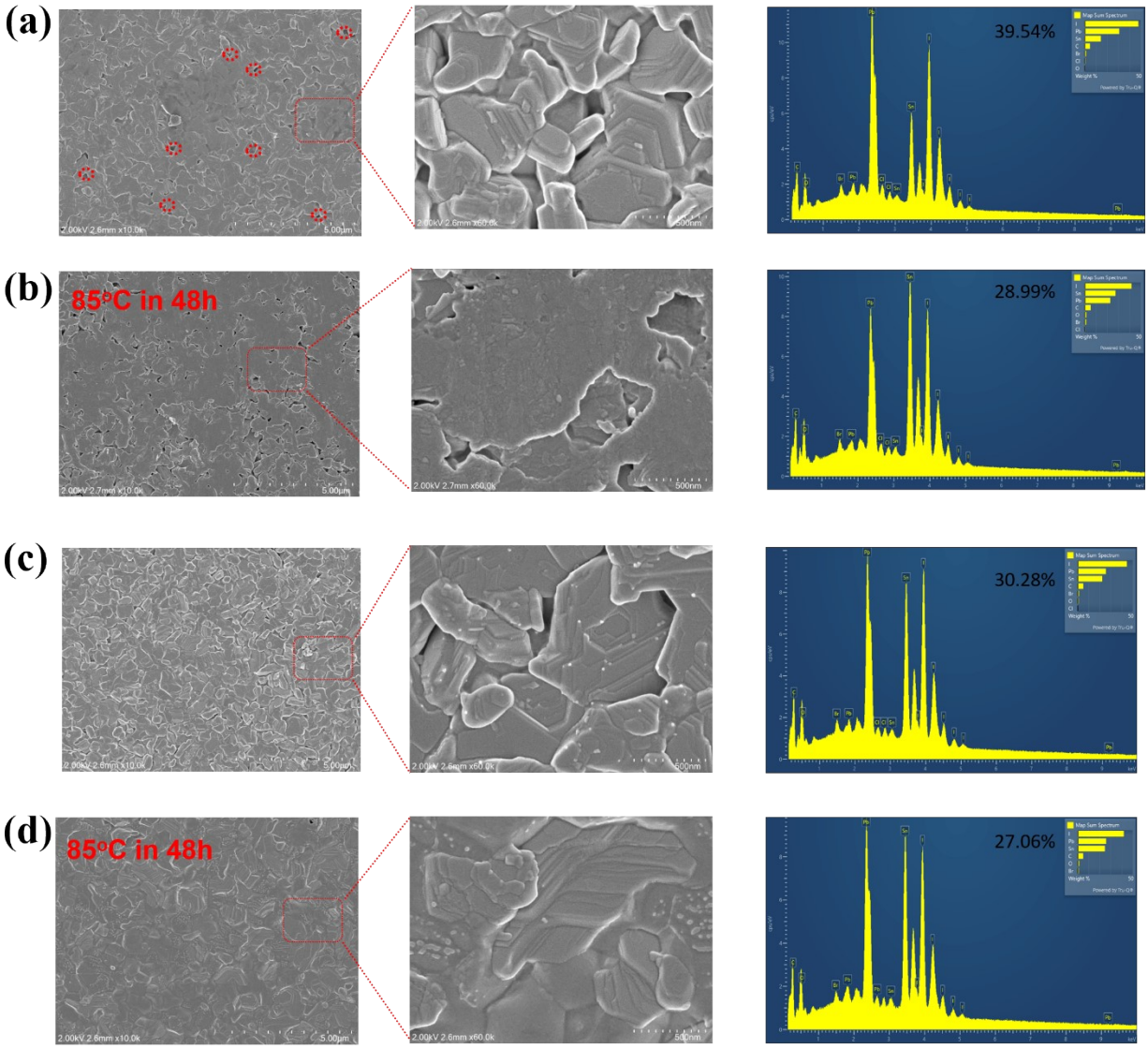

Fig. S20. SEM image and EDX analysis of perovskite coating on (a) SnO_2 at normal condition, (b) SnO_2 at 85°C in 48h, (c) SnO_2-WS_2 at normal condition, and (d) SnO_2-WS_2 at 85°C in 48h.